Supporting Information for

Transition Metal-doped Metal Oxide Nanocrystals: Efficient Substitutional Doping Through a Continuous Growth Process

*Adam W. Jansons,[†] Kristopher M. Koskela,[†] Brandon M. Crockett, & James E. Hutchison**

Department of Chemistry and Biochemistry and Materials Science Institute, University of Oregon, Eugene, Oregon 97403-1253, United States

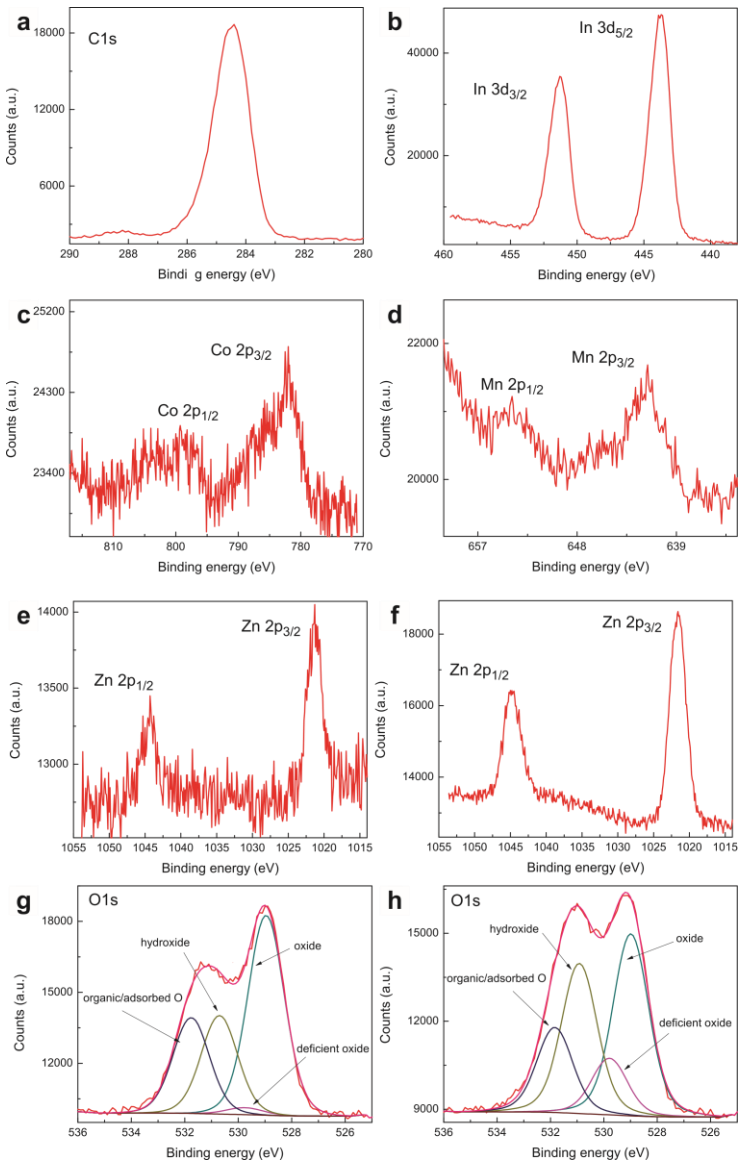

Figure S1. XPS spectra of doped In_2O_3 nanocrystals. Compositions shown in Table 3 of the manuscript are calculated based on integration of the In $3d_{5/2}$ and dopant $2p_{3/2}$ peak. **a**) displays a typical C1s spectra and **b**) a typical In 3d spectra of the doped and undoped nanocrystals. **c**) and **d**) show the Co and Mn 2p spectra from Co: In_2O_3 and Mn: In_2O_3 respectively. **e**) and **f**) display the Zn 2p region of 5% Zn: In_2O_3 and 20% Zn: In_2O_3, respectively. **g**) displays the O1s spectra from 5% Zn: In_2O_3, and **h**) 20% Zn: In_2O_3. The O1s spectra shown in **g** and **h** can be fit to four peaks of the same peak shape and a width of 1.5 eV; the peak at 529.0 eV corresponds to oxide in In_2O_3, the peak 0.7 eV greater corresponds to oxygen deficient/defect oxide, the peak at 530.9 eV corresponds to hydroxide, and the peak at 531.8 eV corresponds to adsorbed oxygen and organic oxygen in the ligand shell.[1–5] The increase in dopant atom concentration likely leads to the increase in oxygen vacancy formation, which is displayed in **g** and **h**. Spectra are referenced to the C1s hydrocarbon peak at 284.5 eV.

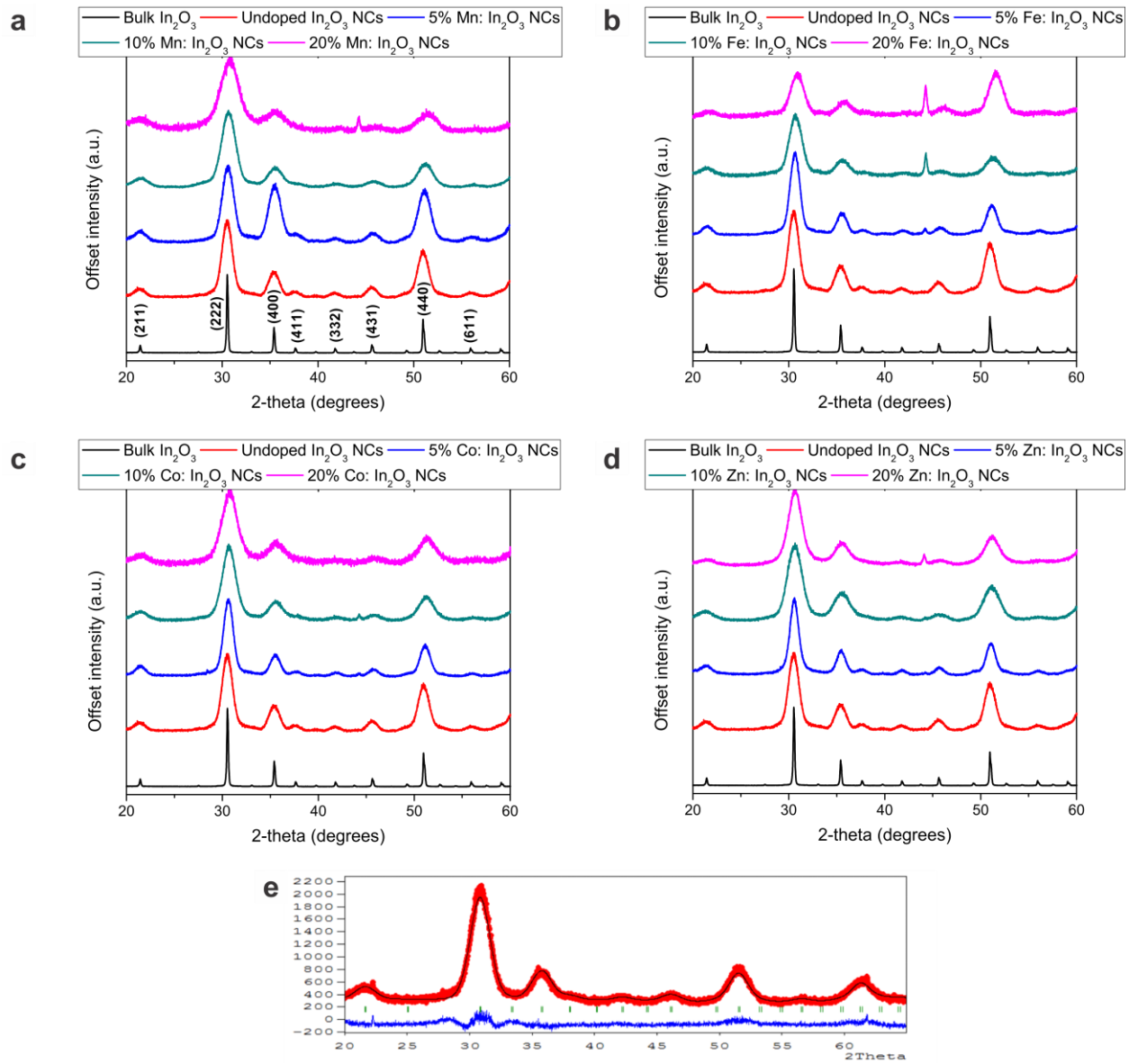

Figure S2. Raw XRD patterns acquired from undoped and doped In_2O_3 nanocrystals at varying dopant concentrations, re-plotted from Figure 2 in the manuscript: **a**) Mn: In_2O_3 **b**) Fe: In_2O_3 **c**) Co: In_2O_3 **d**) Zn: In_2O_3. The peak present at 43.5 ^{o} in some samples is due to the silicon substrate. All acquired patterns match that of cubic In_2O_3 (bulk pattern shown in black in each plot). **e**) Displays a typical Rietveld refinement using Fullprof Suite.[6] Background points were picked by hand, and peaks were fit using a pseudo-Voigt profile. Once scale, zero offsets, and peak shape were refined, lattice parameters were allowed to optimize. In XRD patterns where the substrate peak is present, an exclusion zone in the refinement was added to prevent model optimization from 43-44 ^{o}.

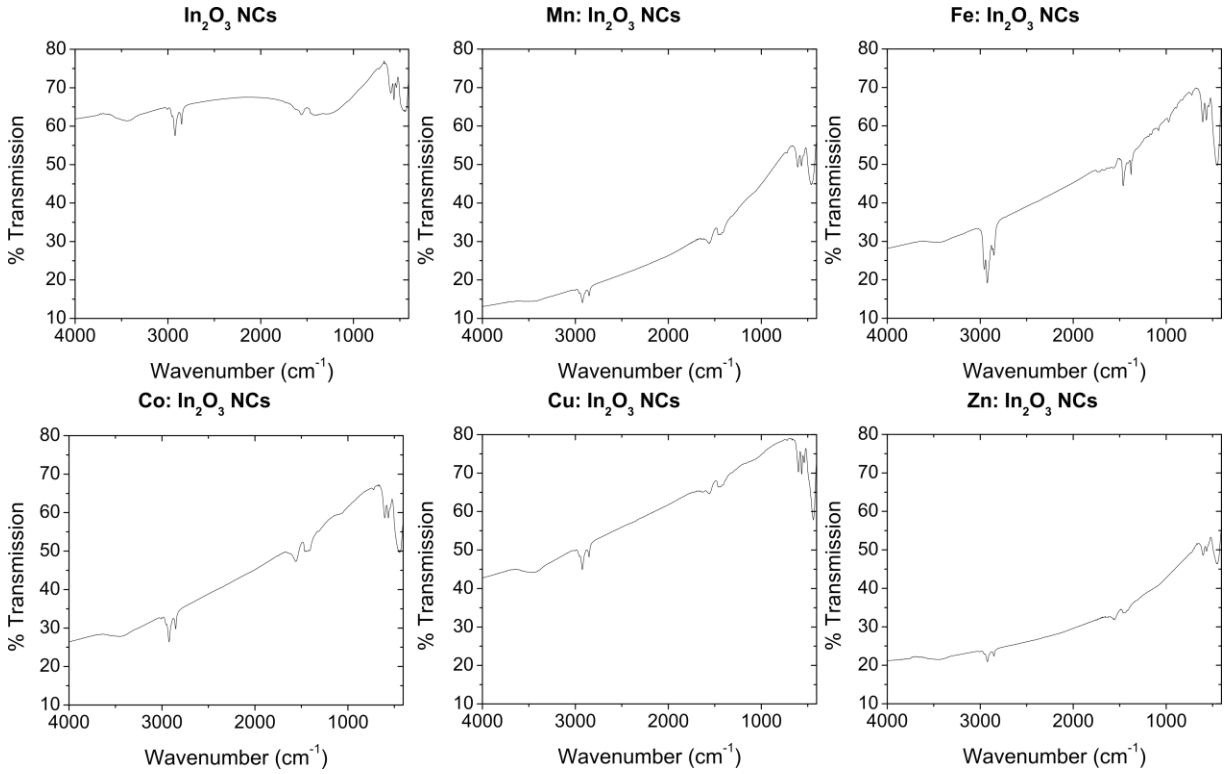

Figure S3. FTIR spectra obtained from undoped and doped In_2O_3 nanocrystals. Unlike the undoped nanocrystals (top left), which display a weak plasmon resonance ~1400 cm^{-1}, the doped nanocrystals display much stronger plasmon absorbances centered at energies > 4000 cm^{-1}. The strong absorbance and the shift of the LSPR to higher energies is an indication of an increased concentration of oxygen vacancy formation.

References:

1. Zai, J., Zhu, J., Qi, R. & Qian, X. Nearly monodispersed $In(OH)_3$ hierarchical nanospheres and nanocubes: tunable ligand-assisted synthesis and their conversion into hierarchical In_2O_3 for gas sensing. *J. Mater. Chem. A* **1,** 735–745 (2013).
2. Lin, A. W. C., Armstrong, N. R. & Kuwana, T. X-ray photoelectron/Auger electron spectroscopic studies of tin and indium metal foils and oxides. *Anal. Chem.* **49,** 1228–1235 (1977).

3. Kim, M.-G., Kanatzidis, M. G., Facchetti, A. & Marks, T. J. Low-temperature fabrication of high-performance metal oxide thin-film electronics via combustion processing. *Nat Mater* **10,** 382–388 (2011).
4. Berthold, T. *et al.* Consequences of plasma oxidation and vacuum annealing on the chemical properties and electron accumulation of In_2O_3 surfaces. *J. Appl. Phys.* **120,** 245301 (2016).
5. Fan, J. C. C. & Goodenough, J. B. X-ray photoemission spectroscopy studies of Sn-doped indium-oxide films. *J. Appl. Phys.* **48,** 3524–3531 (1977).
6. Roisnel, T. & Rodríquez-Carvajal, J. WinPLOTR: a windows tool for powder diffraction pattern analysis. in *Materials Science Forum* **378,** 118–123 (Transtec Publications; 1999, 2001).